ADVANCED MATERIALS INTERFACES
Open Access
www.advmatinterfaces.de

Flat Solenoidal Ice-Binding Proteins as Scaffolds for Solid-Binders

*Robbert J. de Haas, Jannick van Ossenbruggen, Jeffrey van der Hoeven, Roel J. Timmermans, Roderick P. Tas, Ilja K. Voets, and Renko de Vries**

Solid interfacing biomaterials is a crucial aspect of bionanotechnology and important for applications such as biosensing. Because of their potentially large contact area, flat solenoidal proteins are ideal scaffolds for designing proteins binding to surfaces of man-made solids such as minerals, metals, and plastics. To explore this opportunity, a naturally occurring flat solenoidal protein: the *Rhagium inquistor* Antifreeze Protein from the insect Rhagium inquisitor is re-designed. By mutating 4, 6, and 10 out of its 4 × 5 arrays of threonines into arginines, it have arrived at the silica-binding proteins *Ri*SiBP-4, *Ri*SiBP-6, and *Ri*SiBP-10. Variants with increasing numbers of arginines bind stronger to silica, but are also less stable and increasingly difficult to produce. It is found that the RiSiBP-6 variant binds strongly to silica yet still has good stability and easy production. It is shown that sfGFP-RiSiBP-6 fusions allow for the functional display of a monolayer of sfGFP cargo on silica surfaces, suggesting the general usefulness of flat solenoidal proteins as scaffolds for designing solid-binding proteins.

1. Introduction

Placement and activity of biomolecules on solid surfaces is a crucial aspect of bionanotechnology.[1–3] For example in biosensing, antibodies must maintain their native conformation when functionalized on a sensor surface. Such surface functionalization can be achieved via both covalent and noncovalent attachment.[4,5] Both approaches have their strengths and weaknesses: whereas chemical attachment tends to deliver high functionality and stability, processes for chemical attachment can be involved and may require delicate tuning. In contrast, physical attachment can often be achieved in simple (and hence cheap) processes, but tends to deliver lower functionality. As we have argued previously,[6] current methods in protein sequence design may eventually allow for the design of surface-binding proteins that attach themselves to surfaces via physical interactions yet rival the functionality of chemical attachment for surface functionalization.

The best-explored approach for physical attachment of cargo to solid surfaces via protein tags is through the use of short solid-binding peptide (SBPs). Many sequences for SBPs binding to a wide range of materials have been discovered mostly via empirical bio-panning using peptide library screening methods, such as phage display.[7,8] Computer simulations[9] have demonstrated that SBPs typically adopt a wide range of conformations both in solution and at interfaces, making their detailed *de novo* computational design intractable, despite their short sequences.

In contrast, techniques for the *de novo* computational design of proteins with precisely defined folded structures have seen a dramatic development,[10,11] but these have not yet been extensively applied to the design of binders for solid surfaces. One recent example is the *de novo* design of alpha-helical repeat proteins geometrically matched to the potassium ion (K+) sublattice on muscovite mica (001)[12] and more recently the *de novo* design of ice-binding proteins from twist-constrained helices.[13]

Another protein topology with the potential to form extended flat faces that could precisely interact with crystal planes of solid materials, are β-solenoids. So far, a completely *de novo* design of a repetitive β-solenoid has not been reported yet, but there are many natural templates that could be suitable starting points for computational re-design. A particularly suitable class of proteins for this are ice-binding proteins (IBPs)[14,15] with β-solenoid topology, which have extended flat binding surfaces with residues precisely positioned to match with the ice crystal plane to which they preferably bind.[16]

One example is the *RiAFP* antifreeze protein from the insect *Rhagium inquisitor (PDB ID:4DT5)*. This protein has an unusually

R. J. de Haas, J. van Ossenbruggen, J. van der Hoeven, R. J. Timmermans, R. de Vries
Physical Chemistry and Soft Matter
Wageningen University and Research
Stippeneng 4, Wageningen 6708 WE, The Netherlands
E-mail: renko.devries@wur.nl
R. P. Tas, I. K. Voets
Department of Chemical Engineering and Chemistry & Institute for Complex Molecular Systems
Eindhoven University of Technology
De Zaale, Eindhoven 5612 AJ, The Netherlands
The ORCID identification number(s) for the author(s) of this article can be found under https://doi.org/10.1002/admi.202300001.

DOI: 10.1002/admi.202300001

flat beta-solenoid structure, with one side containing the ice-binding residues that consist of an highly ordered matrix of 20 threonine residues that are all pointing in exactly the same direction, and the other side being hydrophilic, containing mostly polar and charged amino acids.[17]

In the absence of stable *de novo* designs for β-solenoid scaffolds, we argue that *Ri*AFP is an ideal scaffold for re-engineering as a flat protein to also bind to other solid surfaces by engineering the threonine residues on the ice-binding site. While for binding to crystalline surfaces (such as ice, or minerals) both precise placement and orientation of binding groups, and an extended flat binding face are crucial, in many other cases (for example amorphous solids, alloys, or plastics), it is especially an extended flat binding interface which will be crucial, and constraints on the placement of binding residues may be less stringent.

As proof of principle, we here consider (amorphous) silica as a model surface, and re-engineer *Ri*AFP to strongly bind to silica (and no longer to ice) by substitution of the ice-binding residues for silica-binding ones. We show that these substitutions can be done based on no rational design because it is quite well-known which amino acid preferentially binds to specific solid surfaces from analysis of the ample SBP sequences. In the case of silica, it is especially arginine that binds strongly, mainly through electrostatic interactions[18,19] which is confirmed by the many silica-binding SBPs that are rich in arginines[3,16—19]. We, therefore, engineer a series *Ri*AFP variants with 4, 6, and 10 arginines replacing ice-binding threonines on the ice-binding face of the *Ri*AFP proteins, generating a series of flat silica-binding proteins *Ri*SiBP-4, *Ri*SiBP-6, and *Ri*SiBP-10. We demonstrate the *Ri*SiBP proteins adsorb as a thin monomolecular layer on silica surfaces, and have an affinity for silica surfaces that increases with their number of designed arginines.

Finally, we demonstrate that cargo fused to the *Ri*SiBP proteins can be functionally displayed on silica surfaces. More generally, we conclude that the rational design of surface binding motifs via residue engineering of proteins with well-defined solid binding surfaces is a successful strategy for rational design of folded and flat surface binding proteins.

2. Results and Discussion

Antifreeze proteins (AFPs), also known as ice-binding proteins (IBPs), have evolved in cold-adapted organisms to bind nucleating ice crystal surfaces to, among others, inhibit formation of damaging ice crystals.[15] Although the precise mechanism of the ice-binding is still opaque, the protein surface residues responsible for ice-binding on the so-called ice-binding site (IBS), have been identified for most AFPs. For *Rhagium inquisitor* AFP (*Ri*AFP) this is a highly ordered flat matrix of 4×5 threonines on one side of its beta-solenoid fold (**Figure 1**). The IBS of *Ri*AFP spans a large atomically flat surface area of $\approx$450 nm^2 where the threonines all protrude in the same plane. Therefore the IBS is ideally suited for rational design of other surface interacting residues.

As proof of principle, we here engineer *Rhagium inquisitor* Silica Binding Proteins (*Ri*SiBPs). To this end, we mutated a varying number of threonine residues on the IBS into positively charged arginine residues, a residue type well known to bind strongly to silica, mainly via electrostatic interactions.[18,19] We thus hypothesize that *Ri*SiBPs with increasing numbers of arginines will have a likewise increasing affinity for silica, and potentially other negatively charged materials.

Based on the *Ri*AFP crystal structure (PDB ID: 4DT5) we design 3 silica-binding variants by respectively selecting 4, 6, and 10 threonines in the 4×5 residue matrix, to be mutated into arginines. In selecting the threonines to be mutated, we aimed at homogeneously distributing arginines over the 4×5 matrix. The resulting proteins are referred to as *Ri*SiBP-4, *Ri*SiBP-6, and *Ri*SiBP-10. For clarity we will refer to the *Ri*AFP wildtype protein as *Ri*SiBP-0, having zero arginines on the ice-binding site. Figure 1 shows cartoon model structures of *Ri*SiBP-0, *Ri*SiBP-4, *Ri*SiBP-6, and *Ri*SiBP-10 generated with Rosetta Design. The ice-binding site is highlighted on *Ri*SiBP-0. The figure also illustrates that the arginine mutations are indeed equally distributed over the IBS.

Next, to increase the solubility and expression of the designed proteins, we included a highly soluble super folder green fluorescent protein (sfGFP) at the N-terminal to make sfGFP-*Ri*SiBP fusion proteins. The sfGFP can be cleaved off

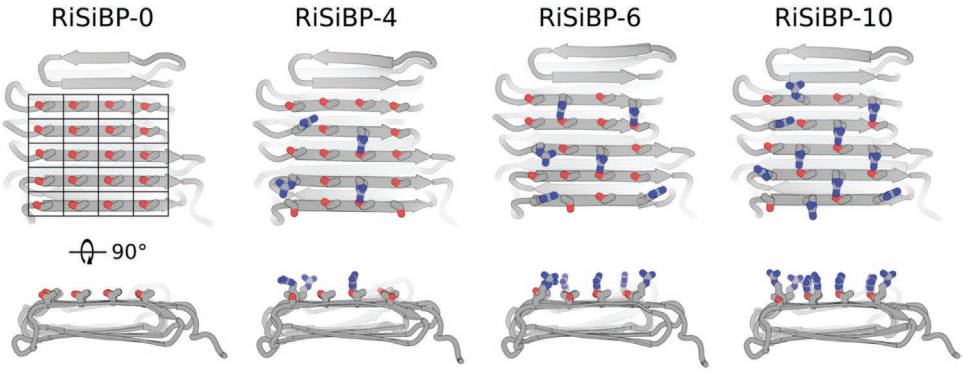

Figure 1. Cartoon models of *Ri*SiBP are shown in XZ (top) and XY (bottom) orientation. The *Rhagium inquisitor* antifreeze protein (PDB ID: 4DT5) is referred to as *Ri*SiBP-0. The putative ice-binding plane is indicated by the raster showing an array of 4×5 threonine residues displayed as sticks. *Ri*SiBP-0 serves as the base scaffold for the design of *Ri*SiBP-4, *Ri*SiBP-6, *Ri*SiBP-10 which have 4, 6, and 10 arginine mutations on the ice-binding plane. Arginine residues are shown as sticks on the sidechain. Oxygen atoms are colored red, and nitrogen atoms are colored blue.

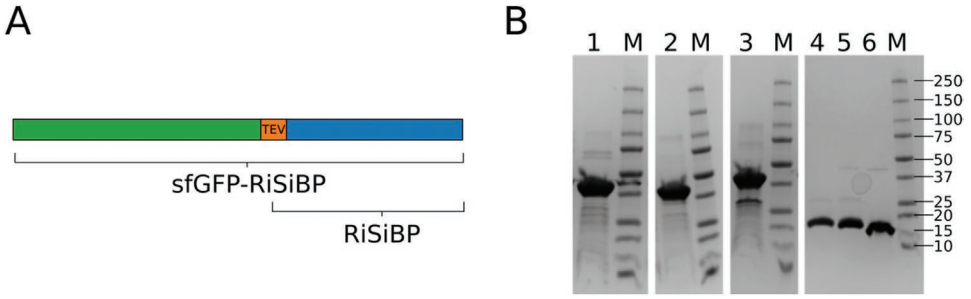

Figure 2. A) Schematic of gene architecture of sfGFP-*Ri*SiBP proteins: sfGFP is fused to *Ri*SiBP via a TEV protease cleavage site. Cleavage of the TEV site led to production of *Ri*SiBP. B) Final purity of proteins used by SDS-PAGE. Lanes: 1) sfGFP-*Ri*SiBP-0, 2) sfGFP-*Ri*SiBP-4, 3) sfGFP-*Ri*SiBP-6, 4) *Ri*SiBP-0, 5) *Ri*SiBP-4, *Ri*SiBP-6, and M) protein standard marker with size in kDa as indicated in the figure.

using a tobacco etch virus (TEV) protease cleavage site which also acts as a spacer between sfGFP and *Ri*SiBP (**Figure 2**A). All designs include a C-terminal hexahistidine tag such that TEV-cleaved *Ri*SiBP can be purified on a Ni-NTA column. Complete sequences for sfGFP-*Ri*SiBP-0, sfGFP-*Ri*SiBP-4, sfGFP-*Ri*SiBP-6, and sfGFP-*Ri*SiBP-10 can be found in Table S1, Supporting Information.

We recombinantly expressed sfGFP-*Ri*SiBP in *E.coli* and purified the proteins using a Ni-NTA column followed by a polishing size-exclusion chromatography (SEC) purification (Figures S1 and S2, Supporting Information). The purified sfGFP-*Ri*SiBP proteins were cleaved with TEV protease, and *Ri*SiBP was isolated using a Ni-NTA column followed by another SEC purification to produce high-purity monomeric *Ri*SiBP (Figure S3, Supporting Information). Figure 2B shows the SDS-PAGE of the final purified proteins used in this study. Lanes 1–3 show final purified sfGFP-*Ri*SiBP-0, sfGFP-*Ri*SiBP-4, and sfGFP-*Ri*SiBP-6. Lanes 4–6 show final purity of *Ri*SiBP-0, *Ri*SiBP-4, and *Ri*SiBP-6. The sfGFP-*Ri*SiBP-10 is not shown, because it expressed poorly and the majority of the expressed protein was found to be insoluble (Figure S1, Supporting Information). Similarly, enforcing 12 arginines on one side of a flat *de novo* designed helical repeat protein (DHR10),[20] the same scaffold used for the *de novo* design of mica binders,[12] also led to poor expression and insoluble protein (Figure S4, Supporting Information). This together demonstrates that independent of the scaffold type, the design of high densities of positive charged can be problematic for soluble expression and folding.

To verify that secondary structure remains the same despite the arginine mutations we obtained circular dichroism (CD) spectra and compared them to the *Ri*SiBP-0 spectrum, for which a crystal structure is available (PDB ID: 4DT5). **Figure 3**A shows the normalized ellipticity for all *Ri*SiBPs overlap with a single minimum at 220 nm, indicating high beta-sheet content. These results are expected considering that *Ri*SiBP-0 is a beta-roll solenoid containing predominantly beta-sheets[17] (Figure 1). To test the influence of the arginine mutations on the scaffold structure stability, a thermal denaturation ramp was performed which shows *Ri*SiBP proteins gradually unfold at high temperature with melting temperatures of $T_m \approx 50°C$ for *Ri*SiBP-0 and *Ri*SiBP-4, and $T_m \approx 38$ °C for *Ri*SiBP-6 (Figure 3B). This demonstrates that incorporation of arginines on the IBS of the *Ri*AFP somewhat reduces the thermal stability of the scaffold, which is not unexpected given the increasingly high density of arginines on the sheets resulting in increased electrostatic repulsion.

Having established that the *Ri*SiBP designs have the correct secondary structure elements and are thermostable at room temperature, we set out to test whether the threonine to arginine substitutions affect ice-binding activity by performing an ice recrystallization inhibition (IRI) assay.[21] AFPs bind to ice owing to the well-ordered presentation of the threonine array, and it has been demonstrated previously that the incorporation of just a few steric mutations with high entropy side chains (such as arginines) on IBS of native AFPs can greatly reduce their IRI activity.[22] In the IRI assay, small ice crystals are nucleated and kept at –8 °C for 45 min in the presence of

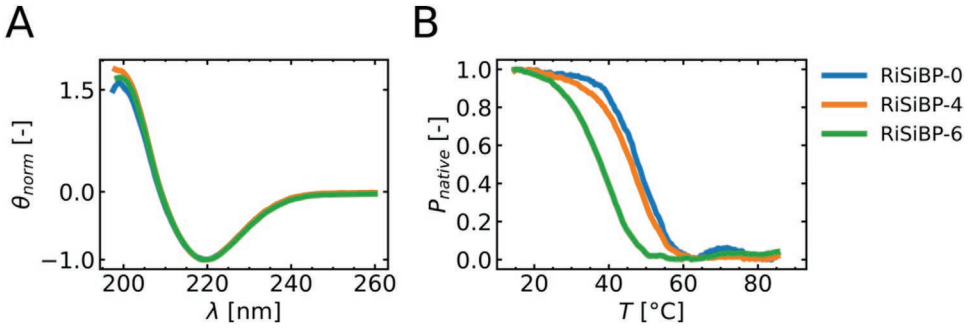

Figure 3. Structure validation and thermal stability of *Ri*SiBP proteins by circular dichroism in PBS. A) Spectra of *Ri*SiBP proteins at $T = 10$ °C. The molar ellipticity is normalized at 220 nm (θ_{norm}). All *Ri*SiBP show a highly similar spectrum typical for proteins rich in beta-sheet content, indicating the protein is folded to the native state. B) thermal melting curves, with on *y*-axis fraction of native protein (P_{native}) at $\lambda = 220$ nm, indicating thermal melting points of 49, 48, and 38 °C for *Ri*SiBP-0, *Ri*SiBP-4, and *Ri*SiBP-6 respectively.

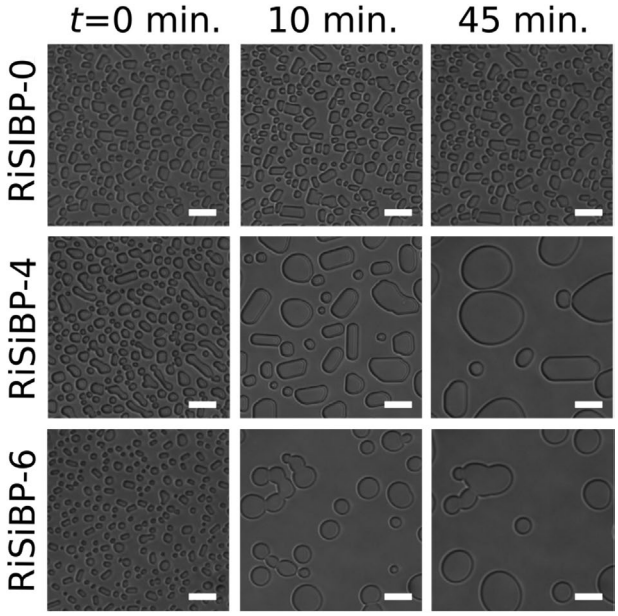

Figure 4. Ice recrystallization inhibition activity of *Ri*SiBP proteins. Experiment performed at *Ri*SiBP concentration 0.2 mg mL^{-1} in PBS + 20% sucrose. ice crystals are rapidly nucleated, and imaged over time at −8 °C. Stills at 0 min, 10 min, and 45 min. are shown. *Ri*SiBP-0 shows no growth of the ice crystals, indicating high activity of ice recrystallization inhibition. *Ri*SiBP-4 and *Ri*SiBP-6 show rapid growth into larger ice crystals over time, indicating decreased ice recrystallization inhibition activity. Scale bar: 50 µm.

0.2 mg mL^{-1} *Ri*SiBP protein. **Figure 4** shows that in the presence of *Ri*SiBP-0, the native *Ri*AFP, ice crystals have not grown in volume over the course of 45 minutes. This crystal growth inhibition is the hallmark of IRI activity. Therefore we confirm *Ri*SiBP-0 is indeed folded to its active native conformation, with its threonine array on the IBS are presented. For the arginine mutants *Ri*SiBP-4 and *Ri*SiBP-6, much faster growth of large ice crystals is observed, confirming that indeed only a few threonine to arginine substitutions on the IBS are enough to reduce the IRI properties of *Ri*SiBP-0.

Having established the native-like folding of *Ri*SiBP proteins, we next test the effect of arginine mutations on *Ri*SiBP scaffold on the binding strength of protein to silica (SiO_2) surface using Quartz Crystal Microbalance Dissipation (QCM-D). In QCM-D, the oscillation frequency of the SiO_2-coated quartz sensor is monitored and changes with adsorbed mass to the surface. Provided dissipation is limited, the adsorbed mass scales linearly with the decrease in oscillation frequency ($\Delta M \propto -\Delta f$) according to the Sauerbrey equation.[23] **Figure 5**A shows QCM-D results for the adsorption of 1 µM of the *Ri*SiBPs, followed by washing with PBS. We find *Ri*SiBP-0 adsorbs to SiO_2 but after washing with PBS, *Ri*SiBP-0 desorbs almost completely, indicating binding is likely due to weak nonspecific interactions. At 1 µM, the kinetics of adsorption of *Ri*SiBP-4 and *Ri*SiBP-6 are similar, and both have a significantly higher plateau adsorption than *Ri*SiBP-0. They differ however in their desorption behavior, with significant desorption during PBS washing for *Ri*SiBP-4, but no desorption during PBS washing for *Ri*SiBP-6.

Figure 5B shows the limiting adsorbed masses per unit area, as estimated from the Sauerbrey equation, for *Ri*SiBP layers versus the concentration at which the layers were formed. A similar mass per unit area is observed for *Ri*SiBP-6 as compared to *Ri*SiBP-4, possibly indicating full monolayer coverage for both cases. The decrease in coverage after prolonged washing with PBS is shown in Figure 5C, again demonstrating that only for *Ri*SiBP-6 there is almost no desorption after prolonged washing with PBS. During QCM-D measurements of *Ri*SiBP-0, *Ri*SiBP-4, and *Ri*SiBP-6, the measured energy dissipation (ΔD) remains well below 1 ppm during the measurements, indicating a only a thin layer of proteins is adsorbed, with no dissipation, thus allowing the use of the Sauerbrey equation for estimating coverages (Figure S5, Supporting Information). The fact that the adsorbed layers are thin and homogeneous is further confirmed by atomic force microscopy (Figure S6, Supporting Information).

Finally, to demonstrate the usefulness of *Ri*SiBP to display functional proteins on silica surfaces, we coat silica nanoparticles (d = 163 nm) with *Ri*SiBP-sfGFP, where the sfGFP is a placeholder for functional proteins one might want to display, such as capture proteins for certain ligands in biosensing. Assuming monolayer coating of the *Ri*SiBP-sfGFP on the silica nanoparticles, we expect a layer height with $h \sim 6$ nm based on the cross-sectional diameter of crystal structures of sfGFP (PDB ID: 2B3P) and *Ri*SiBP (PDB ID: 4DT5) (**Figure 6**A). Using Dynamic Light Scattering (DLS), we measured hydrodynamic diameters of the silica nanoparticles incubated at various concentrations of sfGFP-*Ri*SiBP-0 and sfGFP-*Ri*SiBP-6. From the slight increase in the hydrodynamic diameters of the particles, we are able to estimate layer thicknesses. Indeed, for

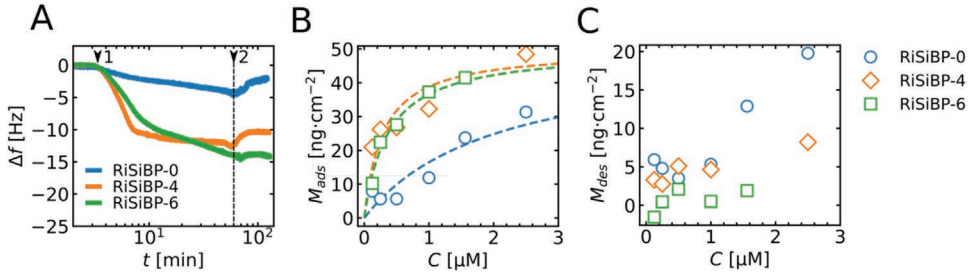

Figure 5. Quartz Crystal Microbalance Dissipation on SiO_2 crystal. A) Frequency shift (Δf) of the 7th overtone over time at a flow speed of 50 µLmin^{-1}. Arrow 1 indicates start of loading of a 1 µM solution *Ri*SiBP-0, *Ri*SiBP-4, and *Ri*SiBP-6 in PBS. Arrow 2 indicates the start of washing with PBS. B) Quantification of adsorbed mass (M_{ads}), calculated using the Sauerbrey equation, after loading phase at various protein concentrations. C) Quantification of desorbed mass per unit area (M_{des}) at various concentrations after the washing phase.

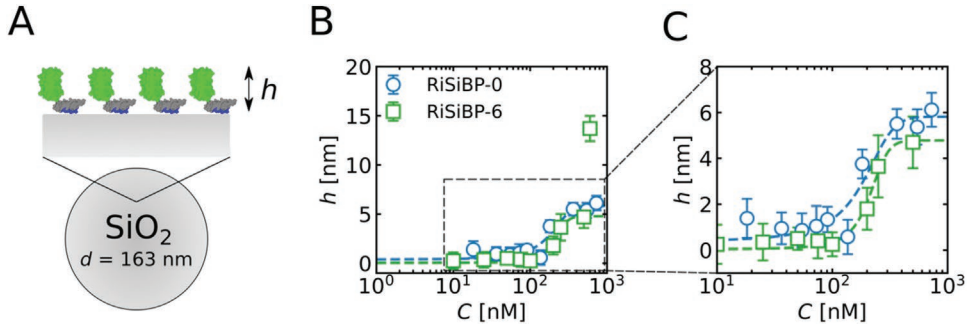

Figure 6. Determination of the layer height of proteins adsorbed to silica nanoparticles (*d = 163 nm*) using dynamic light scattering (DLS). A) schematic representation of the proposed orientation of sfGFP-*Ri*SiBP on a silica nanoparticle. *Ri*SiBP (gray) bind with the arginine-rich plane (blue) to the silica with sfGFP (green) on top. A layer height is expected to be $h \sim 6$ nm based on measurement of crystal structures of sfGFP (PDB ID: 2B3P) and *Ri*SiBP (PDB ID: 4DT5) measured in PyMOL. B) Measured sfGFP-*Ri*SiBP-0 and sfGFP-*Ri*SiBP-6 protein layer height coating on the silica particles as a function of protein concentration. Error bars represent standard deviation of 15 independent measurements. Dotted line represents sigmoid fit to the data. C) Zoom of panel B.

both sfGFP-*Ri*SiBP-0 and sfGFP-*Ri*SiBP-6, at protein concentrations of ≈500 nM, we find a saturation layer thickness $h \sim 6$ nm (Figure 6B-C). For sfGFP-*Ri*SiBP-6 at concentrations >500 nM we observe layer thicknesses $h \sim 13$ nm (Figure 6B). Possibly, multilayer formation at high concentrations can be caused by electrostatic attraction between the *Ri*SiBP-6 and sfGFP domains which have opposite net charges of, respectively, +4 and −8. Overall though, the DLS results confirm monolayer coating of *Ri*SiBP-sfGFP on silica surfaces, with the *Ri*SiBP being bound to the surface and sfGFP pointing into the bulk, as illustrated in Figure 6A.

To test the mobility of sfGFP immobilized on silica surfaces through *Ri*SiBP tagging, we used fluorescence recovery after photobleaching (FRAP). **Figure 7** shows results of FRAP experiments for 1 µM of sfGFP-*Ri*SiBP-0 and sfGFP-*Ri*SiBP-6. For sfGFP-*Ri*SiBP-0 we observe that bleached proteins are gradually being replaced by unbleached ones via exchange with the bulk phase. Exchange via the bulk and hence fluorescence recovery is significantly less for sfGFP-*Ri*SiBP-6, consistent with our earlier experiments that determined that this protein is not easily rinsed away by PBS. For both sfGFP-*Ri*SiBP-0 and sfGFP-*Ri*SiBP-6 the boundary of the bleached area remains sharp, which would not be the case if there was significant in-plane mobility.

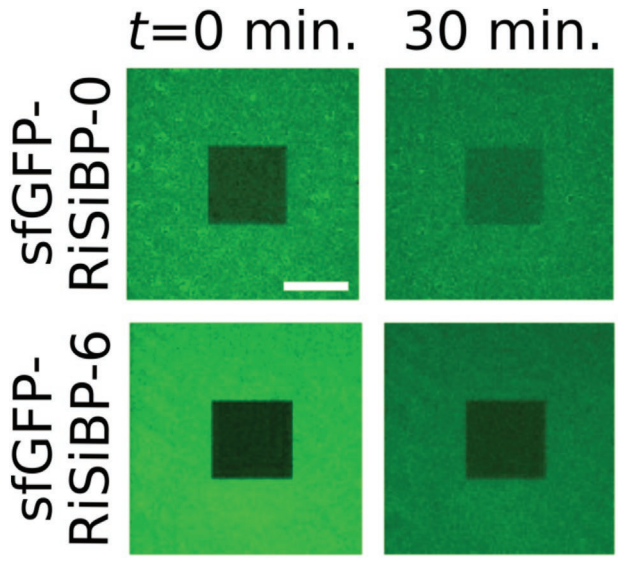

Figure 7. Fluorescence Recovery After Photobleaching (FRAP) on silica in presence of 1 µM sfGFP-*Ri*SiBP-0 and sfGFP-*Ri*SiBP-6. A square in the middle is bleached at $t = 0$ min. by high laser intensity. Stills at $t = 30$ min. after bleaching show recovery of the bleached sfGFP fluorescence in the squares. Some intensity decrease outside the bleach square is also observed due to scan bleaching. Scale bar: 30 µm.

3. Conclusion

To demonstrate the concept of engineering flat solenoid proteins for solid binding, we have designed a series of silica-binding proteins by introducing arginine mutations in a flat solenoid antifreeze protein. The *Ri*SiBP-6, with 6 arginines, binds strongly to silica surfaces, cannot be easily washed away, and has low in-plane mobility when adsorbed. It can be fused with a cargo protein such as sfGFP, and on silica surfaces sfGFP-*Ri*SiBP-6 fusions form a monolayer coating with thickness $h \sim 6$ nm, with the sfGFP being oriented towards the bulk.

Introducing more and more arginines leads to both production problems and lower protein stability. Possibly the introduction of self-assembly, such as fibril formation, could further increase their surface binding strength.[24,25]

In the long run, the *de novo* computational design of flat beta-solenoids could lead to highly stable scaffolds that may tolerate many more surface mutations as compared to native beta-solenoids such as the *Ri*AFP that we investigated here. Such scaffolds would also be suitable for decoration with other surface-binding amino acids, to target other surface materials such as plastics, metals, and other oxides.

By illustrating the concept of the surface engineering of flat solenoid proteins for solid binding using a natural ice-binding protein, we hope to stimulate further work in this area to eventually arrive at highly stable *de-novo* designed beta-solenoid binders for a wide range of solid materials that can be used for bio-material interfacing.

4. Experimental Section

Construct Cloning: Genes encoding sfGFP-*Ri*AFP proteins were codon optimized using codon harmony (version 1.0.0) and obtained as synthetic DNA fragments from Twist Bioscience. The gene fragments were cloned into pET-24(+) vector using restriction digestion with BamHI and XhoI restriction endonucleases (New England Biolabs) and the insert was validated by sequencing.

Protein Expression and Purification: A shaker flask with 1L luberia-broth (LB) medium + 50 mg L^{-1} kanamycin was inoculated from an overnight starter culture of T7-Express *E.coli* containing the expression plasmid. The culture was incubated shaking (125 rpm) until $0.6 < OD_{600} < 0.8$ at 37 °C. Protein expression was induced by 1 mM isopropyl B-D-thiogalactoside (IPTG) and expression was continued at 18 °C overnight. The broth was centrifuged at 6000 x g and the cell pellet was resuspended in cold 30 mL lysis-wash buffer (50 mM Tris-HCl pH 8.0, 400 mM NaCl, 30 mM imidazole) + 1 mM phenylmethylsulfyl fluoride (PMSF) serine protease inhibitor. Cells were lysed by sonication on ice for 7 min. with a 2s on-off duty cycle at 85% amplitude using a Q-sonica Q125 with a CL-18 probe. The lysate was centrifuged at 30000 x g for 30 min. at 4 °C and the clarified supernatant was applied two times on lysis-wash buffer equilibrated Ni-NTA resin with a column volume (CV) of 2 mL. The resin was washed with 25 CVs lysis-wash buffer and eluted with 3 CVs elution buffer (50 mM Tris-HCl pH 8.0, 400 mM NaCl, 300 mM imidazole). The eluate was further purified and buffer-exchanged via size exclusion chromatography (SEC) on an Agilent Infinity II GPC with a Superdex 200 Increase 10/300 GL (GE Healthcare) column in PBS (10 mM phosphate pH 7.4, 137 mM NaCl, 3.7 mM KCl). Fractions containing monomeric sfGFP-*Ri*SiBP proteins were pooled, and protein concentration was determined using a molar extinction coefficient of 23630 $M^{-1}cm^{-1}$ at 280 nm. Purified sfGFP-*Ri*AFP variants were stored at 4 °C.

To purify cleaved *Ri*SiBP protein, the sfGFP-*Ri*SiBP eluate was diluted 20X in cleavage buffer (25 mM Tris-HCl pH 8.0, 100 mM NaCl and 10% glycerol) and ≈3 mg of home-made tobacco etch virus (TEV) protease[26] was added and incubated for 48 hr. at room temperature. The cleaved protein solution was applied to a 2 mL Ni-NTA resin washed with 5 CVs of lysis-wash buffer, and eluted in 3 CVs elution buffer. The eluate was spin concentrated using Amicon 3.5 kDa spin filters (Merck Millipore) and further SEC purified on a Superdex 75 10/300 GL (GE Healthcare) equilibrated in PBS. The monomeric fractions containing *Ri*SiBP protein were pooled and spin concentrated to 1 mg mL^{-1} using a molar extinction coefficient of 1615 $M^{-1}cm^{-1}$ at 280 nm, flash frozen and stored at −20 °C.

Circular Dichroism: Samples were prepared by thawing *Ri*SiBP aliquots on ice and diluting to 0.2 mg mL^{-1} in PBS. A spectropolarimeter J-715 (JASCO Corporation, Japan) to record CD profiles in a quartz cuvette with a 1 mm path length. Spectral scans were averaged over 20 measurements and obtained at 10 °C with a scan rate of 50 nm min^{-1} using a response time of 2s. For thermal denaturation experiments, circularly polarized light was recorded at a fixed wavelength $\lambda = 220$ nm and a response time of 2s at a heating rate of 1°C min^{-1}.

Ice Recrystallization Inhibition: *Ri*SiBP protein aliquots were thawed and diluted to 0.2 mg mL^{-1} in PBS + 20% w/w sucrose. Samples of 2 µL were sandwiched between two precleaned cover slides, which were rapidly frozen at 20 °C min^{-1} to −40 °C to generate tiny polycrystalline crystals using a Linkam LTS420 cold stage attached to a Nikon ECLIPSE Ci-Pol Optical Microscope. The samples were annealed for 90 min at a sample annealing temperature of -8 ± 1 °C. Microphotographs were taken every 2 min using a Lumera3 CCD camera to follow the ice growth over time. Image analysis was done in ImageJ.

Quartz Crystal Microbalance Dissipation: A Q-Sense E4 (Biolin Scientific) QCM-D instrument was used to quantify protein binding to silica. QCM-D quartz sensors coated with SiO_2 (QSX 303, Biolin Scientific) are cleaned according to the manufacturer's instructions. Samples for QCM-D experiments were prepared by diluting freshly thawed *Ri*SiBP protein aliquots in PBS buffer. Prior to the measurements, the instrument was equilibrated with PBS buffer for at least 20 min. at a flow rate of 50 µL min^{-1}. The experiment was started by flushing the sensors with *Ri*SiBP protein at 50 µL min^{-1} for ≈70 min. Next, the flow was briefly stopped, and inlets were switched to PBS buffer to wash the sensors for ≈55 min. Analysis of QCM-D data was done using Q-Sense Dfind software (Biolin Scientific). Experimental observables are the changes in resonance frequency (Δf) and energy dissipation (D). If energy dissipation is small enough, the adsorbed mass per unit area can be (ΔM) estimated from the change in resonance frequency through the Sauerbrey equation:

$$\Delta f = -C\frac{\Delta M}{n} \quad (1)$$

Where n is the number of the odd harmonic (n = 1,3,5, ...) and the numerical prefactor, for a 5 MHz crystal was, per unit area of crystal surface, C = 17.7 ng $(cm^2 \cdot Hz)^{-1}$. The active area of the crystal was 0.2 cm^2.

Dynamic Light Scattering: A ZS-Nano (Malvern, UK) DLS instrument was used to quantify the hydrodynamic diameter of silica nanoparticles coated with sfGFP-*Ri*AFP protein. Light scattering was measured at a fixed angle of 173°, in a quartz cuvette at 20 °C. Samples were prepared by mixing silica nanoparticles of 163 nm diameter (Bang Laboratories), PB (10 mM phosphate pH 7.4), PBS, and sfGFP-*Ri*AFP purified proteins at various concentrations. Prior to measurement, samples were incubated >5 min. at 20 °C. In all samples, the final NaCl concentration was kept constant at 28.2 mM to reduce silica nanoparticle aggregation due to charge screening.[27] Hydrodynamic radii are calculated based on the average of 15 measurements, obtained using the Zetasizer software version 7.13 (Malvern, UK).

Fluorescence Recovery After Photo-Bleaching: Microscopy slides and cover glasses were prepared by plasma cleaning for 2 minutes, and resting for >5 min. Two strips of double-sided tape were stuck on the microscope slide, with the distance just shy of the length of the cover glass (Figure S7, Supporting Information). Between the two strips, a 20 µL droplet containing 1 µM sfGFP-*Ri*SiBP in PBS pH 7.0 was pipetted. The drop was incubated for 2 min, after which the cover glass was placed on top of the tape strips to create a capillary. Through the capillary 150 µL of 1 µM sfGFP-*Ri*SiBP protein was flushed and the ends were sealed with grease to prevent evaporation. The slide was imaged using an oil immersion Plan Apochromat 60x objective (Apo 60x Oil λS DIC N2) with a numerical aperture (NA) of 1.42 on a Nikon Ti confocal microscope with a Nikon C2 laser module. During time-lapse imaging, the focal plane (1.5 AU) of the cover glass was maintained using perfect focus system in the NIS-Element software. Images were recorded at 1 frame per second using a 488 nm laser. Each measurement started with 11 frames obtained at 0.3% laser power to collect a prebleach baseline. Bleaching was done by increasing laser power to 20% and 50% using 488 and 405 nm lasers for 6 seconds. Fluorescence recovery was measured by scanning at 0.3% 488 nm laser for 30 min.

Supporting Information

Supporting Information is available from the Wiley Online Library or from the author.

Acknowledgements

This work was financially supported by a VLAG graduate school fellowship to R.J.dH, the Dutch Research Council to R.P.T (NWO-VENI 202.220), the European Research Council to I.K.V (ERC-2020-CoG 101001965). The authors thank Daniel Ellis and Neil King for introducing the *Ri*AFP structure, Thomas Kodger for assistance with confocal microscopy, and Nicolò Alvisi for assistance with Quartz Crystal Microbalance Dissipation measurements.

Conflict of Interest

The authors declare no conflict of interest.

Data Availability Statement

The data that support the findings of this study are available in the supplementary material of this article.

Keywords

antifreeze proteins, silica-binding proteins, solid-binding proteins, β-solenoid

Received: January 3, 2023
Revised: March 10, 2023
Published online: April 18, 2023

[1] R. A. Vijayendran, D. E. Leckband, *Anal. Chem.* **2001**, *73*, 471.
[2] Y. Wu, C. Chen, S. Liu, *Anal. Chem.* **2009**, *81*, 1600.
[3] C. Liu, D. L. Steer, H. Song, L. He, *J. Phys. Chem. Lett.* **2022**, *13*, 1609.
[4] M. Rabe, D. Verdes, S. Seeger, *Adv. Colloid Interface Sci.* **2011**, *162*, 87.
[5] E. A. Vogler, *Biomaterials* **2012**, *33*, 1201.
[6] N. Alvisi, C. Zheng, M. Lokker, V. Boekestein, R. De Haas, B. Albada, R. De Vries, *Biomacromolecules* **2022**, *23*, 3507.
[7] S. Yun, S. Lee, J. P. Park, J. Choo, E. K. Lee, *J. Biotechnol.* **2019**, *289*, 88.
[8] F. Baneyx, D. T. Schwartz, *Curr. Opin. Biotechnol.* **2007**, *18*, 312.
[9] R. Notman, E. E. Oren, C. Tamerler, M. Sarikaya, R. Samudrala, T. R. Walsh, *Biomacromolecules* **2010**, *11*, 3266.
[10] J. Dauparas, I. Anishchenko, N. Bennett, H. Bai, R. J. Ragotte, L. F. Milles, I. B. Wicky, A. Courbet, R. J. de Has, N. Bethel, *Science* **2022**, *378*, 49.
[11] I. Anishchenko, S. J. Pellock, T. M. Chidyausiku, T. A. Ramelot, S. Ovchinnikov, J. Hao, K. Bafna, C. Norn, A. Kang, A. K. Bera, F. DiMaio, L. Carter, C. M. Chow, G. T. Montelione, D. Baker, *Nature* **2021**, *600*, 547.
[12] H. Pyles, S. Zhang, J. J. De Yoreo, D. Baker, *Nature* **2019**, *571*, 251.
[13] R. J. de Haas, R. P. Tas, D. van den Broek, H. Nguyen, A. Kang, A. Bera, N. P. King, I. Voets, R. de Vries, *bioRxiv* **2022**, 2022.
[14] P. L. Davies, *Trends Biochem. Sci.* **2014**, *39*, 548.
[15] P. L. Davies, J. Baardsnes, M. J. Kuiper, V. K. Walker, D. Hall, M. A. Marahiel, M. Smallwood, D. Smith, T. Haymet, C. Knight, *Philos. Trans. R. Soc., B Biol. Sci.* **2002**, *357*, 927.
[16] S. P. Graethert, M. J. Kulper, S. M. Gagné, V. K. Walker, Z. Jia, B. D. Sykes, P. L. Davies, *Nature* **2000**, *406*, 325.
[17] A. Hakim, J. B. Nguyen, K. Basu, D. F. Zhu, D. Thakral, P. L. Davies, F. J. Isaacs, Y. Modis, W. Meng, *J. Biol. Chem.* **2013**, *288*, 12295.
[18] S. Rauwolf, S. Bag, R. Rouqueiro, S. P. Schwaminger, A. C. Dias-Cabral, S. Berensmeier, W. Wenzel, *J. Phys. Chem. Lett.* **2021**, *12*, 9384.
[19] J. M. Bolivar, B. Nidetzky, *Langmuir* **2012**, *28*, 10040.
[20] T. J. Brunette, F. Parmeggiani, P. S. Huang, G. Bhabha, D. C. Ekiert, S. E. Tsutakawa, G. L. Hura, J. A. Tainer, D. Baker, *Nature* **2015**, *528*, 580.
[21] C. Budke, A. Dreyer, J. Jaeger, K. Gimpel, T. Berkemeier, A. S. Bonin, L. Nagel, C. Plattner, A. L. Devries, N. Sewald, T. Koop, *Cryst. Growth Des.* **2014**, *14*, 4285.
[22] C. P. Garnham, A. Natarajan, A. J. Middleton, M. J. Kuiper, I. Braslavsky, P. L. Davies, *Biochemistry* **2010**, *49*, 9063.
[23] X. Huang, Q. Bai, J. Hu, D. Hou, *Sensors* **2017**, *17*, 1785.
[24] Z. Peng, A. S. Parker, M. D. R. Peralta, K. M. Ravikumar, D. L. Cox, M. D. Toney, *Biophys. J.* **2017**, *113*, 1945.
[25] M. D. R. Peralta, A. Karsai, A. Ngo, C. Sierra, K. T. Fong, N. R. Hayre, N. Mirzaee, K. M. Ravikumar, A. J. Kluber, X. Chen, G. Y. Liu, M. D. Toney, R. R. Singh, D. L. Cox, *ACS Nano* **2015**, *9*, 449.
[26] J. E. Tropea, S. Cherry, D. S. Waugh, *Methods Mol Biol* **2009**, *498*, 297.
[27] J. W. Tavacoli, P. J. Dowding, A. F. Routh, *Colloids Surf. A Physicochem. Eng. Asp.* **2007**, *293*, 167.